

A Two-Layer Network Equivalent With Local Passivity Compensation With Applications to Hybrid Simulations of MMC-Based AC–DC Grids

Dewu Shu , Member, IEEE, Xiaorong Xie , Senior Member, IEEE, Zheng Yan ,
and Venkata Dinavahi , Senior Member, IEEE

Abstract—A frequency-dependent network equivalent (FDNE) is essential to capture wide-band frequency dynamics in the hybrid simulation of large-scale modular multi-level converter based ac–dc grids. The FDNE model must be enforced to be passive, ensuring the numerical stability in time-domain simulations. However, existing passive enforcement techniques based on global optimization perturbations cannot guarantee convergence, accuracy, and efficiency simultaneously. To address the issues, a two-layer FDNE (T-FDNE) model is developed for the ac grids. The two layers, namely, detailed layer and equivalent layer, have their admittances derived by perturbation test and analytical approach, respectively. The passivity of the T-FDNE model is guaranteed by the proposed local passivity compensation technique using auxiliary rational functions. Since no optimization is required and the passivity is enhanced locally, the convergence, accuracy, and efficiency can be improved considerably. By incorporating the T-FDNE model into the interface model of transient (TS) and electromagnetic transient hybrid simulations, wide-band frequency interactions, especially those of very high frequency, can be reflected effectively. The performance (efficiency and accuracy) of the T-FDNE model as well as of the hybrid simulation method has been validated on a modified and practical ac–dc system in China.

Index Terms—Ac/dc grids, electromagnetic transients, frequency-dependent network equivalent, hybrid simulation, local passivity, transient stability.

I. INTRODUCTION

THE hybrid simulation that combines transient stability (TS) and electromagnetic transient (EMT) models is predominantly used for the investigation of interactions between AC and

DC grids [1], [2]. Previously, phasor models at the fundamental frequency were adopted in the TS subsystem [2], [3]. As a result, the interface model between TS and EMT subsystems has a frequency band below the fundamental frequency. It cannot reflect the wide-band frequency interactions between different subsystems, which, however, are necessary in simulating a system integrating many power-electronic devices, for instance, the rapidly developing MMC-based HVDCs [3]. To overcome this issue, the frequency-dependent network equivalent (FDNE) model is added in the interface model of EMT subsystems to represent wide-band frequency interactions of different subsystems [4], [5]. Consequently, the high-frequency interaction of the TS subsystem is represented by the FDNE model and the low-frequency electro-mechanical interaction is modeled as a Thevenin equivalent circuit [2]. The FDNE model and the Thevenin equivalent circuit constitute the overall interface model in each EMT subsystem.

The FDNE model is typically derived as the rational modeling, which is represented in its state-space form [6]. First, the sampled frequency responses of the original AC network are obtained by either numerical simulations or analytical approaches. Then, the frequency responses are curve-fitted as a rational transfer function using rational approximation approaches, such as vector fitting [6]. The obtained rational function is hereafter discretized and state variables of the FDNE model are finally calculated together with the EMT subsystems [7]. However, before the FDNE model or the fitted rational function is calculated in EMT subsystems, the passivity of the FDNE model must be guaranteed; otherwise the derived FDNE model will produce numerically unstable results [6]. Therefore, passivity violation must be carefully identified and removed. The methods available for correcting the model coefficients and recovering the passivity fall into the following categories:

- i) *Semidefinite Programming (SDP) or Positive Real Lemma (PRL) Based Methods* [6], [8], [9]: These methods convert the passivity constrained optimization problem, which is originally non-convex, into a convex optimization problem based on the PRL formula. Consequently, SDP based methods always generate the optimal passive models. However, their computational burden is increased dramatically as the scale of the system expands, due to the fact that the computational complexity is $O(n^2)$, where n is the number of variables [6].

Manuscript received September 7, 2018; revised December 26, 2018, April 1, 2019, and April 27, 2019; accepted May 4, 2019. Date of publication May 22, 2019; date of current version October 24, 2019. This work was supported in part by the National Key Research and Development Program of China under Grant 2017YFB0902800, in part by the National Natural Science Foundation of China under Grant 51737007, in part by SJTU Global Strategic Partnership Fund under Grant 2019 SJTU-KTH, and in part by Shanghai Sailing Program 19YF1423500. Paper no. TPWRS-01345-2018. (Corresponding author: Dewu Shu).

D. Shu and Z. Yan are with the Key Lab of Control and Power Transmission and Conversion, Department of Electrical Engineering, Shanghai Jiaotong University, Shanghai 200240, China (e-mail: shudewu@sjtu.edu.cn; yanz@sjtu.edu.cn).

X. Xie is with the Department of Electrical Engineering, Tsinghua University, Beijing 100084, China (e-mail: xiexr@tsinghua.edu.cn).

V. Dinavahi is with the Department of Electrical Engineering, University of Alberta, Edmonton, AB T6G1H9, Canada (e-mail: dinavahi@ualberta.ca).

Color versions of one or more of the figures in this paper are available online at <http://ieeexplore.ieee.org>.

Digital Object Identifier 10.1109/TPWRS.2019.2918229

Therefore, SDP based methods can only deal with small or medium-sized problems.

- ii) *Perturbation Methods*, e.g., fast residue perturbation (FRP) method [10]: These methods enhance the passivity by perturbing the eigenvalues globally, where the first-order eigenvalue perturbation is modeled as a quadratic programming (QP) optimization problem. However, these methods bring unexpected errors of the frequency range, which does not violate the passivity. As a result, the overall accuracy of the fitted results is reduced. Moreover, the consideration of the whole frequency range in each iteration of the optimization problem would bring convergence and computational issues.
- iii) *Hamiltonian Matrix Based Methods* [11], [12]: With these methods, Hamiltonian matrix is adopted to detect the passivity violation. However, when one of the eigenvalues is perturbed to be stable, other eigenvalues may violate the passivity constraints. The passivity is addressed by increasing iterations of moving eigenvalues. Then the iterations would fail to converge and globally passive solution is not ensured.

In summary, the passivity of the first category is guaranteed but the computation is not efficient. The second category is efficient but it is inaccurate outside the passivity-violated frequency range. The third category would be non-convergent if the eigenvalues are not properly perturbed. Therefore, a guaranteed, accurate and efficient technique is required to enforce the passivity of the FDNE model locally without causing additional convergence and accuracy problems. To achieve this purpose, a two-layer FDNE (T-FDNE) model is proposed and its passivity is enhanced by the local passivity compensation technique. By integrating it into the interface model, a more efficient TS and EMT hybrid simulation is developed. The contributions of this work are threefold:

- i) The T-FDNE model represents the original AC network with two layers, namely, the detailed layer and the equivalent layer. The former captures the wide-band frequency dynamics using the perturbation test; while the latter, as a reduced-order equivalent rational function, improves the efficiency considerably.
- ii) The passivity of the T-FDNE model is guaranteed by the proposed local passivity compensation technique using auxiliary rational functions. The convergence, accuracy and efficiency is significantly improved because the passivity is enhanced locally. Noticeably, no global optimization based perturbations are required.
- iii) By incorporating the T-FDNE model into the interface model, the hybrid simulation is able to investigate wide-band frequency (especially high-frequency) interactions between TS and EMT subsystems.

The rest of the paper is organized as follows: Section II introduces the framework of the proposed TS and EMT hybrid simulation, which incorporates the T-FDNE model. Section III elaborates the T-FDNE model. Section IV illustrates the local passivity compensation technique for the T-FDNE model.

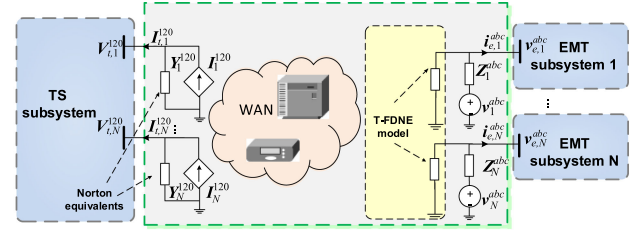


Fig. 1. Framework of the EMT and TS hybrid simulation.

Section V examines the performance of the proposed method on a modified and practical AC/DC system in China. Brief conclusions are finally drawn in Section V.

II. FRAMEWORK OF TS AND EMT HYBRID SIMULATION

Fig. 1 demonstrates the framework of TS and EMT hybrid simulation, where the whole system is partitioned into an AC-grid based TS subsystem and a DC-grid based EMT subsystem. Traditional generators and AC grids (including transmission lines and transformers) are contained in the TS subsystem. To capture the nonlinear and frequency-dependent dynamics, DC grids are included in one or more EMT subsystems. The interactions between different subsystems are reflected by the interface models, where the FDNE model is used to reflect wide-band frequency interactions. In the TS subsystem, the interface model is represented by three-sequence Norton equivalents, including equivalent currents I_j^{120} , $j = 1, 2, \dots, N$ and equivalent admittances Y_j^{120} , $j = 1, 2, \dots, N$ [2]. In contrast, the interface model with each EMT subsystem is represented by the parallel connections of a T-FDNE model and a Thevenin equivalent circuit that comprises three-phase equivalent voltages, v_j^{abc} , $j = 1, 2, \dots, N$ and equivalent impedances Z_j^{abc} , $j = 1, 2, \dots, N$. The Thevenin equivalent circuit is adopted to capture low-frequency electro-mechanical interactions while the T-FDNE model is adopted to represent high-frequency interactions. The parameters of interface models are transmitted through the communication network based on Socket or shared memory techniques.

A. Interface Model in the EMT Subsystem

As shown in Fig. 1, the interface model with the j th EMT subsystem is a combination of a T-FDNE model and a paralleled Thevenin equivalent circuit. The former will be elaborated later in Section III. For the latter, its impedances Z_j^{abc} , $j = 1, 2, \dots, N$ are derived by Gaussian elimination [2] and its three-phase voltages v_j^{abc} , $j = 1, 2, \dots, N$ are calculated by

$$v_j^l = V_j^l \cos(\delta + \theta_j^l), l = a, b, c, \quad (1)$$

where v_j^l , θ_j^l are the magnitude and angle of the interface voltage of each phase, which are given by the TS simulation; $\delta = \int_0^t \omega dt$ stands for the integral of angular speed.

With the interface models updated for each subsystem, the dynamic equations of the j th EMT subsystem as well as its

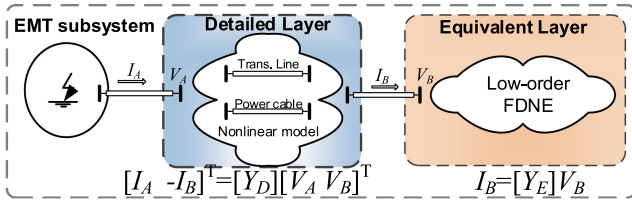


Fig. 2. Structure of the two-layer FDNE.

interfaces are written as

$$\begin{cases} \frac{dx_{emt,j}^{abc}}{dt} = \mathbf{F}_{1,j}(x_{emt,j}^{abc}, i_{e,j}^{abc}), \\ \frac{di_{e,j}^{abc}}{dt} = \mathbf{F}_{2,j}(x_{emt,j}^{abc}, i_{e,j}^{abc}, v_j^{abc}, x_{fdne}), \\ \frac{dx_{fdne,j}}{dt} = \mathbf{F}_{3,j}(i_{e,j}^{abc}, x_{fdne,j}), \end{cases} \quad (2)$$

where $x_{emt,j}^{abc}$, $x_{fdne,j}$ are the state variables of the j th EMT subsystem and the T-FDNE model, respectively; $\mathbf{F}_{1,j}$, $\mathbf{F}_{2,j}$ and $\mathbf{F}_{3,j}$ are state-space equations, of which the details can be found in [2] and [6].

B. Interface Model in the TS Subsystem

The interface models in the TS subsystem are represented as the three-sequence Norton equivalents, i.e., the equivalent currents I_j^{120} , $j = 1, 2, \dots, N$ and the equivalent admittance Y_j^{120} , $j = 1, 2, \dots, N$. The interface voltages and currents in the phasor form are calculated in each EMT subsystem. Then, they are transformed into the three-sequence domain, or $I_{t,j}^{120}$, $V_{t,j}^{120}$. The Norton currents are derived by

$$I_j^{120} = I_{t,j}^{120} + Y_{t,j}^{120} V_{t,j}^{120}. \quad (3)$$

Based on the proposed interface model, as well as the TS models of AC grid and EMT models of DC grid, the hybrid simulation is realized in a coordinated and decoupled way. Its general procedure and time sequence can be found in our previous work [2] and would not be repeated here.

III. TWO-LAYER FREQUENCY-DEPENDENT NETWORK EQUIVALENT

In this work, the FDNE model is developed in three steps:

- Step 1: Obtain the admittance-frequency response of AC grid, or $Y_{fdne}(\omega_i)$, $\omega_i = 2\pi f_i$, $i = 1, 2, \dots, N$ in an accurate and efficient way.
- Step 2: Express $Y_{fdne}(\omega)$ as a linear combination of rational functions by minimum least-square fitting.
- Step 3: Guarantee the passivity of the FDNE model based on the proposed local passivity compensation technique.

This section discusses the fulfillment of Step 1 using the two-layer FDNE (T-FDNE) model. Steps 2 and 3 will be detailed in Section IV.

A. Derivation of the Detailed Layer With Perturbation Test

As shown in Fig. 2, the T-FDNE model divides the original AC grid into two layers, namely the detailed layer and the equivalent layer. Generally, long transmission lines or power cables are

included in the detailed layer, of which the admittance matrix can be written as:

$$Y_D(\omega) = \begin{bmatrix} Y_{AA}(\omega) & Y_{AB}(\omega) \\ Y_{BA}(\omega) & Y_{BB}(\omega) \end{bmatrix}, \quad (4)$$

where subscript A , B stand for the multi ports connected to the EMT subsystem and the equivalent layer, respectively.

In order to capture the wide-band frequency dynamics, the excitation injection test is adopted to calculate the admittance matrix at different frequencies. Different from the procedures in [13], we inject components at different frequencies simultaneously into the boundary buses of the detailed layer. As voltages and currents of specific frequencies at the boundary bus are extracted through Fourier analysis independently, the admittance matrix can be calculated at each frequency:

$$Y_D(\omega) = \sum_{i=1}^N Y_D(\omega_i) \delta(\omega - \omega_i), \omega_i = 2\pi f_i, i = 1, 2, \dots, N, \quad (5)$$

where N is the number of samples; f_i is the i th frequency of sampling; $Y_D(\omega_i)$ is the admittance matrix at ω_i , which is calculated as the ratio of boundary current and voltage phasors in frequency domain. It should be noted that long transmission lines or power cables are included in the detailed layer, where the frequency dependent impedance matrix is obtained by measurement. This is because it is difficult to calculate the frequency dependent impedance matrix of long transmission lines or power cables in an analytical way.

B. Derivation of the Equivalent Layer With Analytical Approach

Since high-frequency dynamics of the EMT subsystem do not travel far into the TS subsystem, the equivalent-layer model focuses on the low-frequency behavior. It is represented as a reduced-order equivalent rational function by analytical approaches. Specifically, all components in the equivalent layer are represented by their simplified EMT models. For instance, a transmission line is modelled as a pi-section circuit; transformers are modelled as leakage inductances and generators as transient inductances. Then the admittance matrix of the equivalent layer, or $Y_E(\omega)$, can be obtained by eliminating all the nodes except the boundary buses with the Gaussian elimination [6].

By combining the admittances of the two layers, the admittance of the TS subsystem is derived as [14]:

$$Y_{fdne}(\omega) = Y_{AA}(\omega) - Y_{AB}(\omega)[Y_{BB}(\omega) + Y_E(\omega)]^{-1}Y_{BA}(\omega), \quad (6)$$

where $Y_{AA}(\omega)$, $Y_{AB}(\omega)$, $Y_{BA}(\omega)$, and $Y_{BB}(\omega)$ are the four individual elements of $Y_D(\omega)$.

IV. LOCAL PASSIVITY COMPENSATION TECHNIQUE FOR FDNES

A. Minimum Least-Square Fitting Based on SK Iterations

The curve-fitting procedure of FDNE model as a rational transfer rational function in s domain or $Y_{fdne}(s)$ is formulated

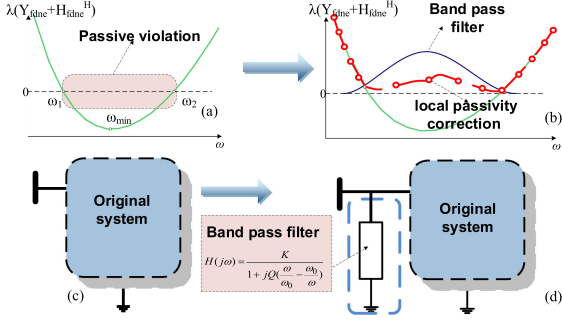


Fig. 3. Proposed local passivity compensation technique for calculating T-FDNEs.

into a least-square problem [6]:

$$\min \sum_{j=1}^l \rho_j \left| \tilde{Y}_{fdne}(s) - Y_{fdne}(s_j) \right|^2, \rho_j > 0 \quad (7)$$

where

$$\tilde{Y}_{fdne}(s) = \tilde{n}(s) / \tilde{d}(s), \quad (8)$$

$$\tilde{n}(s) = c + \sum_{j=1}^r \frac{\phi_j}{s - \lambda_j}, \tilde{d}(s) = 1 + \sum_{j=1}^r \frac{\varphi_j}{s - \lambda_j}. \quad (9)$$

The parameters in (7) are obtained by the Sanathanan and Koerner (SK) iterations, a particular case of which is named the vector fitting technique in [15]. When the eigenvalues $\lambda_j, j = 1, 2, \dots, r$ are determined, other parameters in $\mathbf{x} = [\phi_1, \dots, \phi_r, c, \varphi_1, \dots, \varphi_r]^T$ are hereafter calculated by the solution to the least-square problem $\Delta \mathbf{A} \mathbf{x} = \mathbf{b}$, where ξ_1, \dots, ξ_l are sampled values; $\Delta = \text{diag}\{\rho_j\}_{j=1}^l$, $\mathbf{b} = [-\tilde{Y}_{fdne}(\xi_1), \dots, -\tilde{Y}_{fdne}(\xi_l)]^T$, $\mathbf{x} = [\phi_1, \dots, \phi_r, c, \varphi_1, \dots, \varphi_r]^T$ and

$$\mathbf{A} = \begin{bmatrix} \frac{1}{\xi_1 - \lambda_1} & \dots & \frac{1}{\xi_1 - \lambda_r} & 1 & \frac{-\tilde{Y}_{fdne}(\xi_1)}{\xi_1 - \lambda_1} & \dots & \frac{-\tilde{Y}_{fdne}(\xi_1)}{\xi_1 - \lambda_r} \\ \vdots & & & & & & \vdots \\ \frac{1}{\xi_l - \lambda_1} & \dots & \frac{1}{\xi_l - \lambda_r} & 1 & \frac{-\tilde{Y}_{fdne}(\xi_l)}{\xi_l - \lambda_1} & \dots & \frac{-\tilde{Y}_{fdne}(\xi_l)}{\xi_l - \lambda_r} \end{bmatrix}. \quad (10)$$

With (7)-(10) solved, the obtained state-space form of $Y_{fdne}(s)$ can be denoted as $\sum_o : (A_o, B_o, C_o, D_o)$ [10].

B. Local Passivity Compensation Technique

To avoid numerical stability issues, the T-FDNE model must be enforced to be passive. Ideally the passivity of the violated $\lambda[Y_{fdne}(\omega) + Y_{fdne}^H(\omega)]$ should be enhanced merely at specific frequencies. However, the traditional global perturbation techniques, for instance the FRP technique, improve the passivity at the cost of changing the global parameters. Although the passivity might be enhanced by perturbing the eigenvalues iteratively, errors of the frequency range, which does not violate the passivity, would be unexpectedly enlarged. To reduce the fitting errors in (7) and guarantee the passivity simultaneously, the local passivity compensation technique is proposed in this work. Its principle is illustrated in Fig. 3. An auxiliary rational function behaves like a band-pass filter to increase the value of $\lambda[Y_{fdne}(\omega) + Y_{fdne}^H(\omega)]$ at violated frequencies to enhance the

passivity. Simultaneously, their values at other frequencies drop immediately without enlarging the fitting errors in (7).

The proposed local passivity compensation technique essentially involves the following three steps:

Step 1: Determine the frequency range of passivity violation: Calculate $\lambda[Y_{fdne}(\omega) + Y_{fdne}^H(\omega)]$ at each frequency and detect the frequency range which violates the passivity, for example, the frequency range $[\omega_1, \omega_2]$ in Fig. 3. And the minimum (most negative) eigenvalue is denoted as λ_{min} at ω_{min} . Therefore, passivity within the frequency range $[\omega_1, \omega_2]$ should be corrected by using the auxiliary rational function.

Step 2: Derive the auxiliary rational function for a single port (single input single output case, SISO): As shown in Fig. 3, a band-pass filter is added to make the eigenvalues of $\lambda[Y_{fdne}(\omega) + Y_{fdne}^H(\omega)]$ be positive within $[\omega_1, \omega_2]$. Meanwhile the curve at other frequency range is almost unchanged. The rational function of the band pass filter is represented as

$$H(j\omega) = \frac{K}{1 + jQ\left(\frac{\omega}{\omega_0} - \frac{\omega_0}{\omega}\right)}. \quad (11)$$

Clearly, the peak of $|H(j\omega)|$ appears at the frequency of ω_0 with a magnitude of K . In order to compensate the magnitude of $\lambda[Y_{fdne}(\omega) + Y_{fdne}^H(\omega)]$ at ω_{min} , ω_0 in (11) is set as ω_{min} , or $\omega_0 = \omega_{min}$. The magnitude of the $H(j\omega)$ at ω_0 should be large enough to make the eigenvalues of $\lambda[Y_{fdne}(\omega) + Y_{fdne}^H(\omega)]$ well above the real axis, which is achieved by letting

$$K = \alpha \frac{\lambda_{min}}{2}, \alpha > 1. \quad (12)$$

The parameter Q in (11) is determined by the following inequalities:

$$\omega_1 > \omega_l = \omega_0 \sqrt{1 + \frac{1}{4Q^2}} - \frac{\omega_0}{2Q}, \quad (13)$$

$$\omega_2 < \omega_u = \omega_0 \sqrt{1 + \frac{1}{4Q^2}} + \frac{\omega_0}{2Q}, \quad (14)$$

where ω_l, ω_u are lower and upper cutting-off frequencies of the band-pass filter, respectively.

Step 3: Derive the auxiliary rational function for multi ports (multiple input multiple output case, MIMO): In the multi-port cases, a series of band-pass filter is added to update the eigenvalues of $\mathbf{H}(s) + \mathbf{H}^H(s)$, where $\mathbf{H}(s)$ is the transfer function matrix. A straightforward way is to make the update transfer matrix be diagonal with identical diagonal entries, that is,

$$\mathbf{H}(s) = \begin{bmatrix} H_1(s) & & & \\ & H_2(s) & & \\ & & \ddots & \\ & & & H_n(s) \end{bmatrix} \equiv \text{diag}\{H_1(s), H_2(s), \dots, H_n(s)\} \quad (15)$$

where n denotes the number of the ports. And each $H_i(s)$ is implemented according to Step 2.

The state-space realization can also be written as (16) with matrices therein replaced by

$$A_f = \text{blkdiag}(A_1, \dots, A_n), B_f = \text{blkdiag}(B_1, \dots, B_n),$$

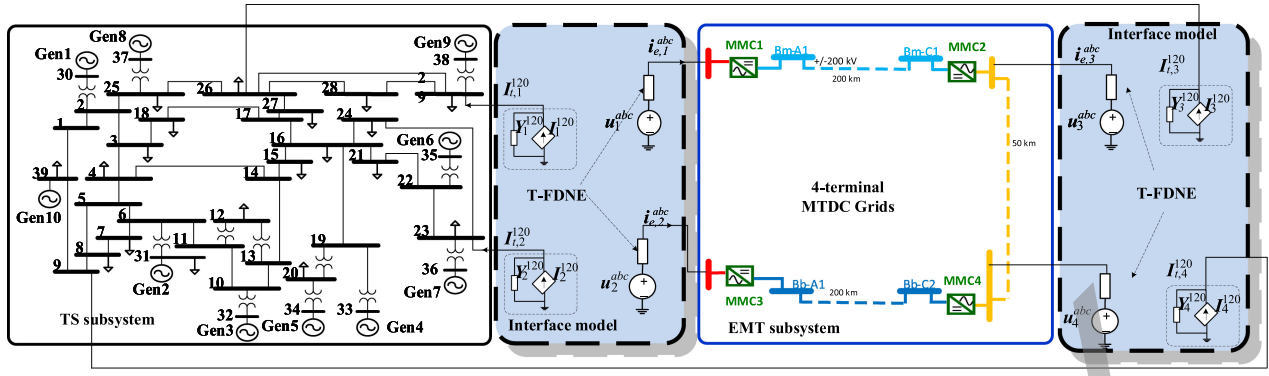


Fig. 4. A four-terminal MMC based MTDC system with IEEE 39 AC system .

$$C_f = \text{blkdiag}(C_1, \dots, C_n), D_f = \text{blkdiag}(D_1, \dots, D_n) \quad (16)$$

where (A_i, B_i, C_i, D_i) is the state-space representation of $H_i(s)$; 'blkdiag' denotes the Matlab function to construct block diagonal matrix from input arguments.

The representation in (16) is controllable and observable if (A_i, B_i, C_i, D_i) is controllable and observable. Therefore, it is the minimal realization of this system. In other words, every compensation enlarges the system size by $2n$ for regular violation, where n denotes the number of ports.

Step 4: Transform the band-pass filter in (15) into the state-space form, or $\sum_f : (A_f, B_f, C_f, D_f)$. Then the complete state-space equations of the T-FDNE model are derived as $\sum_T : (A_T, B_T, C_T, D_T)$, with

$$A_T = \begin{bmatrix} A_o & \\ & A_f \end{bmatrix}, B_T = \begin{bmatrix} B_o \\ B_f \end{bmatrix}. \quad (17)$$

$$C_T = [C_o \quad C_f], D_T = D_o + D_f. \quad (18)$$

The proposed local passivity compensation technique has the following advantages:

- i) Since the compensations of passivity-violated frequencies are fixed locally, the loss of accuracy due to passivity enforcement is minimized.
- ii) Convergence problem is avoided by adding auxiliary rational functions to enhance the passivity.
- iii) As no optimization procedures are required, the proposed technique is more efficient than traditional optimization-based techniques.

Thanks to these distinct features, the passivity of the T-FDNE model is enhanced by the local passivity compensation technique. After that the state-space equations of the T-FDNE model are discretized and realized as an independent module in the EMT subsystems, the simulation of which can fully reflect wide-band frequency interactions between TS and EMT subsystems for large-scale AC/DC grids [10].

V. NUMERICAL TESTS AND VALIDATION

In this section, the proposed method as well as the traditional method is applied to two test systems, i.e., the modified AC/DC system and a practical AC/DC system in China, to evaluate the performance of the hybrid simulation incorporating the T-FDNE

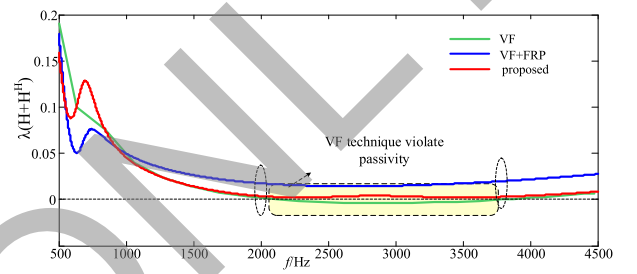


Fig. 5. Eigenvalue plot of $H + H^H$ by different methods of Bus 26.

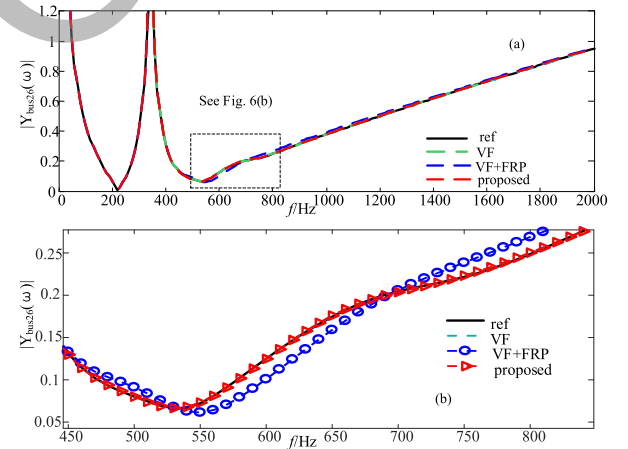


Fig. 6. Comparative results of the fit to $|Y_{bus26}(\omega)|$.

model. Case studies on the first system focus on AC fault scenarios; while the second case focuses on DC fault scenarios, where hybrid HVDC breakers (HHB) are inserted to isolate DC faults. In both cases, the T-FDNE model is included in the interface model to reflect the wide-band frequency interactions between TS and EMT subsystems. The simulation time-steps of TS/EMT subsystems are 5 ms/20 μ s, respectively. Meanwhile, simulation results obtained with a unanimous time-step of 20 μ s are used as the high-fidelity reference values.

A. The Modified AC/DC System

The modified AC/DC system (see Fig. 4) is used to evaluate the performance of the proposed hybrid simulation method

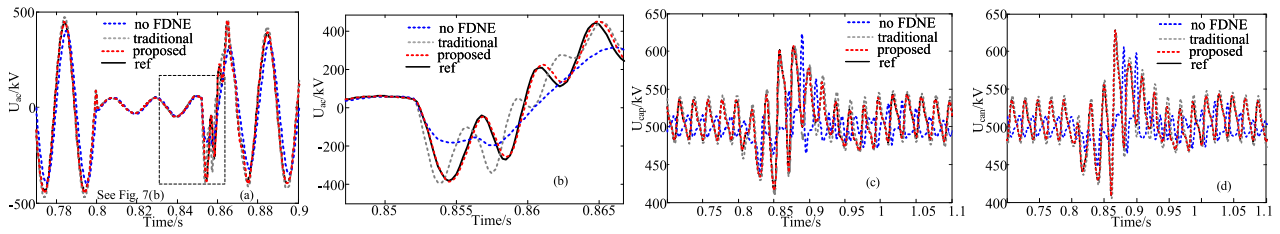


Fig. 7. Interface AC voltages and capacitor voltages of MMC 1.

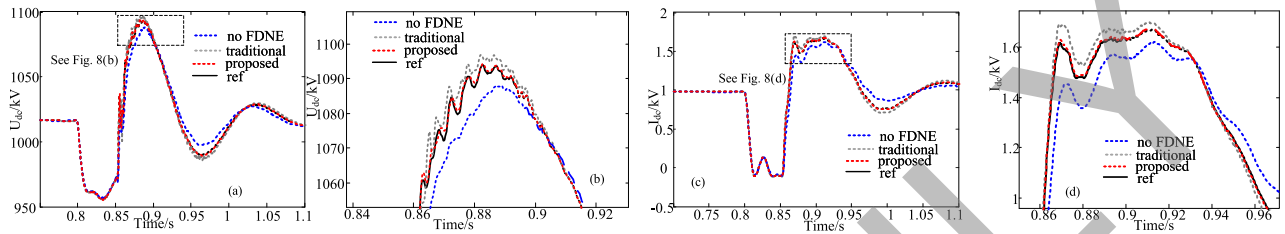


Fig. 8. DC voltages and DC currents of MMC 1.

TABLE I
COMPARISONS OF DIFFERENT FITTING METHODS

Methods	VF	traditional (VF+FRP)	proposed
Consuming time	11.23s	23.57s	11.26s
RMS average error/p.u	1.32E-04	1.52E-03	1.12E-04
Passivity	Non-passive	passive	passive

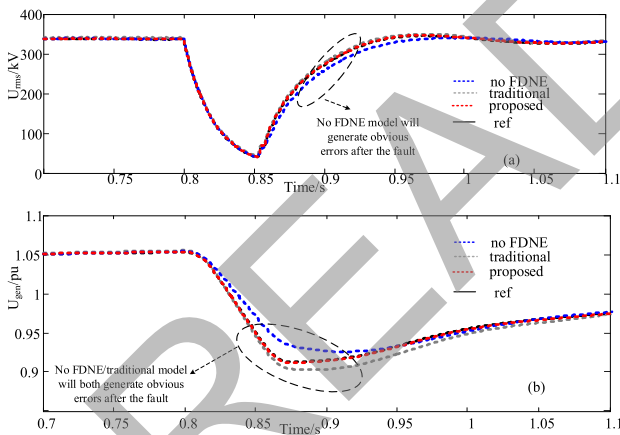


Fig. 9. (a) Voltages of interface bus 26; (b) terminal voltages of the generator at bus 26.

with the proposed T-FDNE model. Its AC grid is the IEEE 39-node system and the DC grid, which comprises a four-terminal ± 500 kV MMC-MTDC system, is adapted from the Zhangbei project in China. Each MMC has 250 half-bridge sub-modules in a single arm. MMC2 regulates the DC voltage while other MMCs control power flows.

1) *Simulation Results of Interface Model With Two Ports:* For the first scenario, MMC2 and MMC4 are connected to Bus 26 and Bus 9 respectively, where MMC1 and MMC3 are directly connected to an ideal voltage source behind the Thevenin

impedance. This is the so-called scenario of the two-port based interface model. In this scenario, the proposed T-FDNE model is compared with the one obtained with the VF + FRP technique. First, the admittance-frequency responses at the boundary buses of 9 and 26 are obtained by our T-FDNE model. Then, the T-FDNE model is curve-fitted. The poles and residues before/after adding the band-pass filter are detailed also in Appendix. As can be seen, most of the eigenvalues remain the same after adding band-pass filter. Moreover, there are additional poles and residues, making the FDNE model passive. Specifically, for Bus 26, the results obtained using the proposed method, vector fitting (VF) and traditional method (VF + FRP) are compared in Figs. 5–6 and Table I. The reference curve, referring to the actual admittance-frequency response of Bus 26, or $Y_{bus26}(\omega)$, is also displayed in Fig. 6.

Fig. 5 indicates that only the VF + FRP and the proposed technique ensure the passivity; while the VF technique fails. Fig. 6(b) shows that traditional method (VF + FRP) introduces significant errors within the frequency range of 400–800 Hz. In contrast, the results given by the proposed technique are consistent with the reference curve, indicating satisfied accuracy. Besides the improvement in passivity and accuracy, Table I has also demonstrated that the proposed technique is as efficient as the vector fitting technique, but faster than the traditional technique. The reasons for efficiency improvement are twofold: i) There is no additional time-consuming optimization problems to be solved. ii) The parameters of band-pass filters can be easily derived based on (11)–(14).

Then, the simulation results of our proposed model are compared with those of the full-scale EMT model (marked as “ref”), the hybrid simulation without the FDNE model (marked as “no FDNE”). The FDNE model of the traditional method is the interface model with higher number of ports, where each port is represented by a three-phase frequency dependent impedance matrix. The frequency dependent impedance matrix is obtained by the traditional vector fitting+ fast residue perturbation

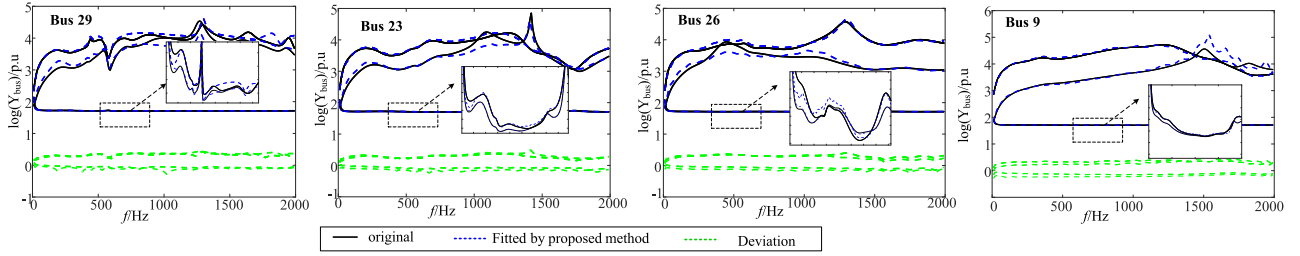


Fig. 10. Fitted admittance matrix of different interfaces .

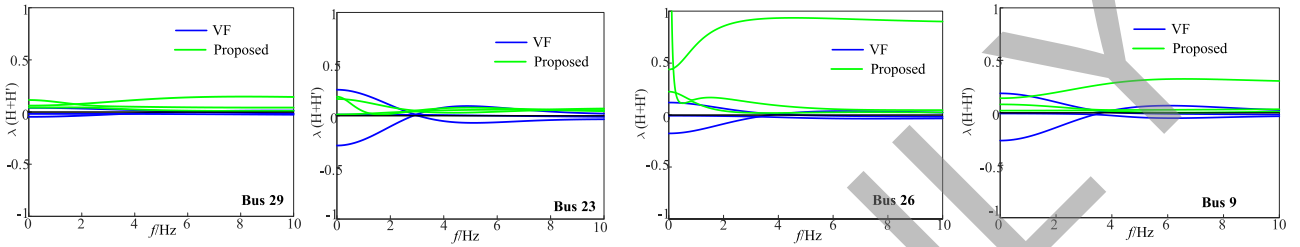
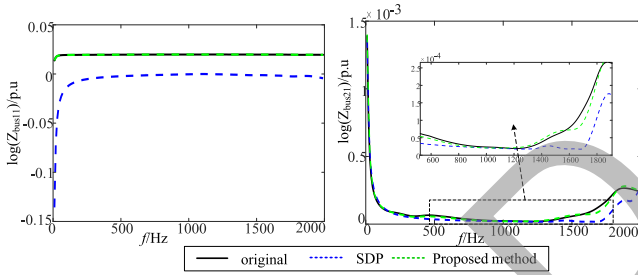
Fig. 11. Eigenvalue plot of $H(s) + H^H(s)$ of different interfaces in Fig. 10.

Fig. 12. Fitted admittance matrix of different interfaces by different methods.

(VF + FRP) technique (marked as “traditional”). As shown in Figs. 7–8, the proposed method is the most accurate; while the traditional method and “no FDNE” method cause significant errors. Note that the zoomed-in curves in Fig. 7 indicates that the high-frequency dynamics of the interface AC voltages cannot be captured accurately by the “no FDNE” method, especially after the clearance of the fault. As a result, the errors of DC voltages and currents are enlarged. Even unwanted phase shift errors are introduced in the capacitor voltages. Such observations confirm the need of an accurate FDNE model for the investigation of high-frequency dynamics of different subsystems.

Fig. 9 shows voltages of interface bus 26 as well as terminal voltages of the generator connected at bus 26. A good consistence can be observed between results of our proposed method and the reference curve. However, both the traditional method and the “no FDNE” method have obvious simulation errors, especially during the fault period.

2) Simulation Results of Interface Model With Four Ports:

In this scenario, four MMC stations are connected to Bus 29, Bus 23, Bus 26, Bus 9, respectively. For each interface, the T-FDNE model is represented as a three-phase frequency dependent impedance matrix. It should be noted that for the hybrid TS

TABLE II
COMPARISONS OF DIFFERENT FITTING METHODS

Methods	VF	SDP	proposed
Consuming time/s	6.15	21.15	6.3
RMS average error/p.u	1.5e-2	11.7	1.7e-2
Passivity	Non-passive	passive	passive

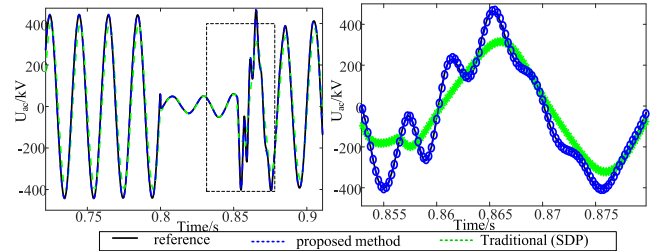


Fig. 13. Interface AC voltages by using different methods.

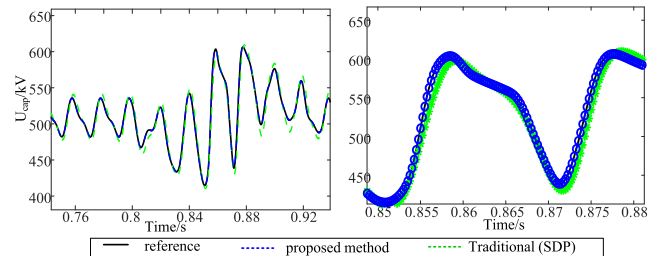


Fig. 14. Capacitor voltages by using different methods.

and EMT simulations, the high-frequency interactions between different ports of interface model are extremely weak and thus can be ignored. Consequently, the proposed FDNE model in our cases supports the interface model with higher number of ports,

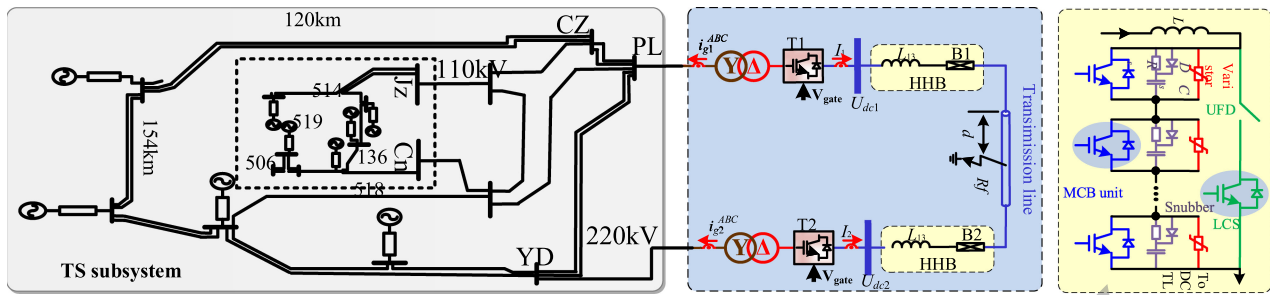


Fig. 15. A practical AC/DC system .

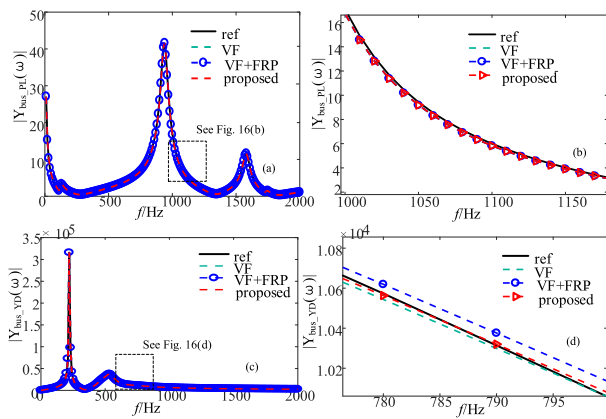


Fig. 16. Comparative results of the admittances at the boundary buses.

where each port is represented by a three-phase frequency dependent impedance matrix. As can be seen from Figs. 10–11, the proposed local compensation method can fit the frequency-impedance matrix curves very well and obtain the desired passive FDNE model; while the vector fitting technique fails. More importantly, Fig. 12 and Table II demonstrate the fitted results by the proposed method is significantly more accurate than those by the traditional SDP method. As shown in Table II, the proposed method is even more accurate and efficient than the traditional SDP method. When the dimension of the fitted frequency dependent impedance matrix increases, the efficiency of the SDP method will drop dramatically, or even non-convergent issues will occur. As evidently shown from Figs. 13–14, the proposed T-FDNE model can achieve accurate simulation results as expected; while the simulation results by using the SDP technique show significant errors.

3) *Discussion on the FDNE Model for the Hybrid TS and EMT Simulations:* For the FDNE model of our proposed hybrid simulation method, the couplings between different interfaces are neglected. Actually, the reason why the couplings between different interfaces depends on the choice of the boundary and the partitioning strategy between AC and DC subsystems. The partitioning position for our proposed method is chosen according to the following rules in order to neglect the couplings between different interfaces:

- 1) The mutual impedances between different interfaces are so large that the couplings are too small to impact

the simulation accuracy. Normally, the electric distances between interface buses are large enough. As a result, the high-frequency interactions between interfaces can be neglected.

- 2) The selected interface bus has the least number of connected buses. In other words, the electric connections between interfaces are very weak.

Based on the above-mentioned partitioning strategy, the proposed hybrid simulation method based on our T-FDNE model can achieve quite satisfied accuracy and efficiency. Moreover, our method adopts the interface model with higher number of ports, where each port is represented by a three-phase frequency dependent impedance matrix. For our special case of the MMC based AC/DC grids, the couplings between different interfaces are so weak that can be neglected. As a result, the electric connection between MMC converters and the adjacent AC buses is weak. On the other hand, for those interfaces which are strongly connected, we can change the partitioning position to resolve this issue.

B. Applications to a Practical AC/DC System in China

The target system is adapted from a practical AC/DC system that comprises a two-terminal MMC based ± 200 kV MTDC grid. As depicted in Fig. 15, the MTDC grid is connected to the neighboring AC buses, namely PL and YD. The controllers and their protection systems are consistent with the practical controllers of Zhoushan Project in China. To operate the MTDC grid, Converter no.1 maintains the DC voltage and the other converter regulates power flows. According to Zhoushan Project, hybrid HVDC breakers (HHBs) are inserted at two ends of the DC lines to isolate the dc faults and quickly restart the DC grids. Each HHB contains six parts: current limiting inductor L , residual current breaker (RCB), ultrafast disconnector (UFD), load commutation switch (LCS), metal oxide varistor (MOV), and main circuit breaker (MCB) with the snubber circuit. The operations of HHBs can be referred to [16].

In our method, the whole system is partitioned into different TS and EMT subsystems, respectively. The majority of AC grids is partitioned in the TS subsystem to guarantee the efficiency. In order to capture the detailed and accurate responses of its controllers and protection systems, the MTDC grid has to be placed in the EMT subsystem. As the interface models, the proposed T-FDNE model is included to reflect the high-frequency dynamics

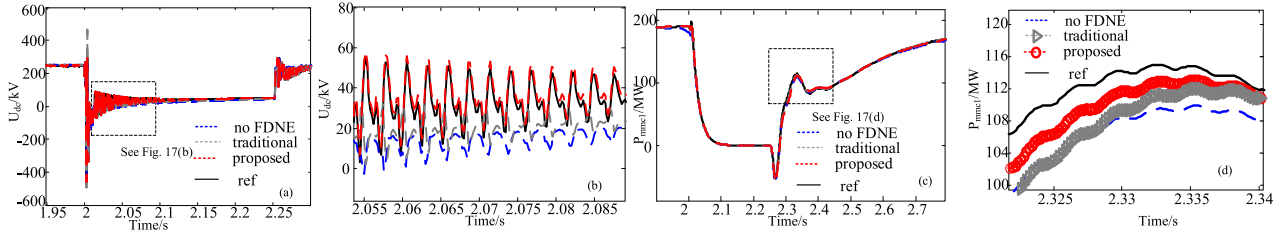


Fig. 17. AC voltages and capacitor voltages of MMC 1.

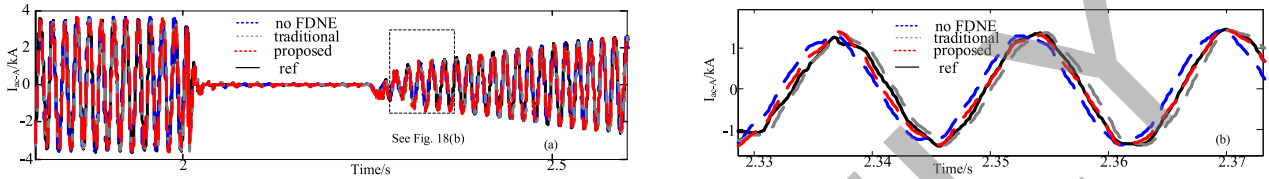


Fig. 18. DC voltages and DC currents of MMC 1.

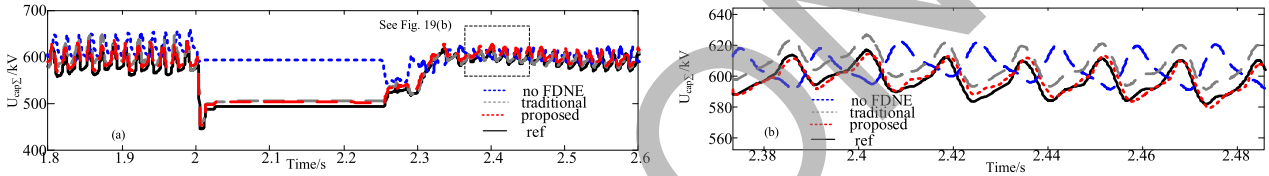


Fig. 19. Sum of capacitor voltages of MMC1.

TABLE III
COMPARISONS OF DIFFERENT FITTING METHODS

Bus		VF	VF+FRP	proposed
PL	Consuming time/s	0.67	5.89	0.67
	RMS average error/p.u.	8.729	8.729	8.715
	passivity	passive	passive	passive
YD	Consuming time/s	0.47	5.78	0.48
	RMS average error/p.u.	22.13	5.158	5.148
	passivity	Non-passive	passive	passive

among TS and EMT subsystems, so that the interactions among different components, for instance, generators, converters and networks, can be simulated precisely.

Similarly, the admittance-frequency responses of boundary buses are curve-fitted by the T-FDNE model in the frequency range of 0-2000Hz. Typical results are shown in Fig. 16 and Table III. It is observed that that VF + FRP and the proposed method can guarantee the passivity of Bus YD; while the VF method fails. However, the zoomed-in curves in Fig. 16(b, d) and Table III show that the proposed method is the most accurate and efficient. It can be concluded that the proposed T-FDNE model does improve the passivity, accuracy and efficiency simultaneously.

A pole-to-ground fault is simulated. It happens at $t = 2.0s$ in the middle of the dc line connecting converters T1 and T2. The fault resistance is 0.01Ω . Figs. 17–19 display the obtained DC quantities, AC quantities and capacitor voltages, respectively.

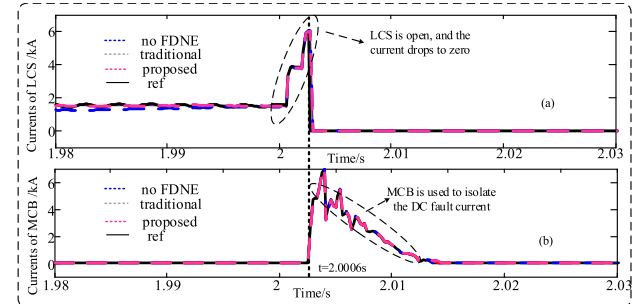


Fig. 20. Currents of LCS and MCB.

As shown in Figs. 17 and 20, as the DC voltage drops dramatically following $t = 2.0 s$ the fault current grows immediately. The HHB takes action at about $2.0006s$ due to the time delay between the HHB and the faulting point. The latter is 400 km away from MMC1. Once the fault current exceeds the threshold, the LCS inside the HHB is opened and the fault current is commutated to the paralleled circuit loop of MCB. Then, the UFD is opened within 2ms to isolate the LCS from the faulting line. With the UFD in its open position, the MCB breaks the fault current with the aid of the fast-switching power electronic devices. The disconnecting circuit breakers B1 and B2 is switched off hereafter and the faulted line is isolated from the MTDC grid. Finally, when the dc fault is cleared, the whole system is restarted at $t = 2.2 s$, as shown in Fig. 17.

TABLE IV
CHARACTERISTICS OF DIFFERENT SIMULATION METHODS

Models/ Method	Detailed EMT	Hybrid simulations	
	simulation (ref)	Traditional FDNE model	T-FDNE model
Total time/s	8230	490	432

As shown in Figs. 17–19, the proposed method is of the highest accuracy; while the “no FDNE” case produces significant errors. The comparisons between Figs. 17 and 18 indicate that the accuracy enhancement in AC quantities is more evident than that of DC quantities. The reasons lie in that: i) The FDNE model improves the precision of interfaces and thus the accuracy of both AC and DC quantities become better. ii) The accuracy of interfaces has larger impacts on the AC quantities than on the DC quantities. It is also indicated in Fig. 19 that the capacitor voltages provided by the proposed method overlap the reference curve; while the “no FDNE” results have obvious errors. In other words, the accuracy of sub-module dynamics, such as capacitor voltages, is also sensitive to the accuracy of interfaces. Therefore, when high-frequency power electronic devices such as MMCs are integrated into the EMT subsystems, their wide-band dynamics are sensitive to the waveforms of adjacent AC quantities. Then an additional FDNE model with improved accuracy is very necessary.

C. Comparisons of Simulation Efficiency

Table IV illustrates the total CPU time consumed by the different models/methods. As is shown, the proposed T-FDNE based hybrid simulation has achieved a speed-up of 20 times over the detailed EMT simulation. With its improved accuracy taken into account, the proposed method offers an accurate and efficient option for analyzing very large-scale AC/DC grids.

VI. CONCLUSION

In this paper, a two-layer frequency-dependent network equivalent (T-FDNE) model is proposed and integrated into the hybrid simulation. The admittances of the T-FDNE model are curve-fitted and their passivity is enhanced by the local passivity compensation technique. Since no optimization is required and the passivity is enhanced locally, the convergence, accuracy and efficiency can be greatly improved. Therefore, the wide-band frequency interactions, especially those of high frequency, can be captured accurately and efficiently in simulating large-scale MMC based AC/DC grids.

The performance of the proposed method has been fully validated on practical AC/DC systems. Simulation results have demonstrated that:

- i) The passivity of the T-FDNE model is guaranteed by the local passivity compensation technique. Besides this, it has achieved a speedup of more than 50 times over the VF technique and the accuracy of non-passive boundary buses has improved by 5 times.
- ii) The proposed method is more accurate than other hybrid simulation methods with no or traditional FDNE models.

Noticeably, the accuracy enhancement in AC quantities is more evident than that of DC quantities.

- iii) The proposed method has achieved a speedup of 20 times over the reference curve, indicating it has achieved a satisfied efficiency.

APPENDIX

POLES AND RESIDUES BEFORE/AFTER ADDING BAND-PASS FILTER

Before adding band-pass filter		After adding band-pass filter	
Poles	Residues	Poles	Residues
-28.0	-455	-28.0	-455
-3.73e3	-1.4e5	-3.73e3	-1.4e5
-38.4±1.3e3i	2.4e5±2.8e5i	-38.4±1.3e3i	2.4e5±2.8e5i
-8.6±1.4e3i	4.9e6±2.8e5i	-8.6±1.4e3i	4.9e6±2.8e5i
-798±1.5e3i	1.5e5±1.2e5i	-798±1.5e3i	1.5e5±1.2e5i
-365±3e3i	5.6e6±3.9e6i	-365±3e3i	5.6e6±3.9e6i
-554.6±3.3e3i	-1.2e6±9.7e5i	-554.6±3.3e3i	-1.2e6±9.7e5i
-207.4±3.3e3i	4.5e6±1.8e6i	-207.4±3.3e3i	4.5e6±1.8e6i
-576.2±4.6e3i	1.1e6±6.2e5i	-576.2±4.6e3i	1.1e6±6.2e5i
-1.8e3±6.2e3i	1.8e5±4.8e5i	-1.8e3±6.2e3i	1.8e5±4.8e5i
-100±1.02e4i	1.3e4±1.1e4i	-100±1.02e4i	1.3e4±1.1e4i
		-3e4+2e3i	0.03+577i
		-3e4-2e3i	0.03-577i

REFERENCES

- [1] J. Shair *et al.*, “Overview of emerging sub-synchronous oscillations in practical wind power systems,” *Renew. Sustain. Energy Rev.*, vol. 108, pp. 159–168, 2019.
- [2] D. Shu, X. Xie, Q. Jiang, Q. Huang, and C. Zhang, “A novel interfacing technique for distributed hybrid simulations combining EMT and transient stability models,” *IEEE Trans. Power Del.*, vol. 33, no. 1, pp. 130–140, Mar. 2017.
- [3] X. Meng and L. Wang, “Interfacing an EMT-type modular multilevel converter HVDC model in transient stability simulation,” *IET Gen. Transmiss. Distrib.*, vol. 11, no. 12, pp. 3002–3008, Sep. 2017.
- [4] X. Lin, A. M. Gole, and M. Yu, “A wide-band multi-port system equivalent for real-time digital power system simulators,” *IEEE Trans. Power Syst.*, vol. 24, no. 1, pp. 237–249, Feb. 2009.
- [5] Y. Liang, X. Lin, A. M. Gole, and M. Yu, “Improved coherency-based wide-band equivalents for real-time digital simulators,” *IEEE Trans. Power Syst.*, vol. 26, no. 3, pp. 1410–1417, Jul. 2011.
- [6] Y. Z. Hu, W. C. Wu, A. M. Gole, and B. M. Zhang, “A guaranteed and efficient method to enforce passivity of frequency-dependent network equivalents,” *IEEE Trans. Power Syst.*, vol. 32, pp. 2455–2463, May 2017.
- [7] B. Gustavsen and H. M. Jeewantha De Silva, “Inclusion of rational models in an electromagnetic transients program: Y-Parameters, Z-parameters, Sparameters, transfer functions,” *IEEE Trans. Power Del.*, vol. 28, no. 2, pp. 1164–1174, Mar. 2013.
- [8] C. P. Coelho, J. Phillips, and L. M. Silveira, “A convex programming approach for generating guaranteed passive approximations to tabulated frequency-data,” *IEEE Trans. Comput.-Aided Design Integr. Circuits Syst.*, vol. 23, no. 2, pp. 293–301, Feb. 2004.
- [9] Y. Hu, W. Wu, and B. Zhang, “A semidefinite programming model for passivity enforcement of frequency-dependent network equivalents,” *IEEE Trans. Power Del.*, vol. 31, no. 1, pp. 397–399, Feb. 2016.
- [10] B. Gustavsen, “Fast passivity enforcement for pole-residue models by perturbation of residue matrix eigenvalues,” *IEEE Trans. Power Del.*, vol. 23, no. 4, pp. 2278–2285, Oct. 2008.
- [11] S. Grivet-Talocia and A. Ubolli, “On the generation of large passive macro-models for complex interconnect structures,” *IEEE Trans. Adv. Packag.*, vol. 29, no. 1, pp. 39–54, Feb. 2006.

- [12] S. Grivet-Talocia, "Passivity enforcement via perturbation of Hamiltonian matrices," *IEEE Trans. Circuits Syst. I, Reg. Papers*, vol. 51, no. 9, pp. 1755–1769, Sep. 2004.
- [13] M. Matar and R. Iravani, "A modified two-layer network equivalent for the analysis of electromagnetic transients," *IEEE Trans. Power Del.*, vol. 25, no. 1, pp. 434–441, Jan. 2010.
- [14] X. Nie, Y. Chen, and V. Dinavahi, "Real-time transient simulation based on a robust two-layer network equivalent," *IEEE Trans. Power Syst.*, vol. 22, no. 4, pp. 1771–1781, Nov. 2007.
- [15] C. K. Sanathanan and J. Koerner, "Transfer function synthesis as a ratio of two complex polynomials," *IEEE Trans. Autom. Control*, vol. AC-9, no. 1, pp. 56–58, Jan. 1963.
- [16] G. Liu, F. Xu, Z. Xu, Z. Zhang, and G. Tang, "Assembly HVDC breaker for HVDC grids with modular multilevel converters," *IEEE Trans. Power Electron.*, vol. 32, no. 2, pp. 931–941, Feb. 2017.



Dewu Shu (M'18) received the B.Sc. and Ph.D. degrees in electrical engineering from Tsinghua University, Beijing, China, in 2013 and 2018. He is currently the Tenure-Track Assistant Professor in electrical engineering with Shanghai Jiaotong University, Shanghai, China. His research interests include multirate EMT/TS simulations, parallel, and distributed computing.



Xiaorong Xie received the B.Sc. degree from Shanghai Jiao Tong University, Shanghai, China, in 1996 and the Ph.D. degrees from Tsinghua University, Beijing, China, in 2001. From 2001 to 2005, he was a Lecturer with the Department of Electrical Engineering, Tsinghua University, where he has been an Associate Professor since 2005. His current research interests include power system analysis and control, and flexible ac transmission systems.



Zheng Yan received the B.S. degree from Shanghai Jiao Tong University, Shanghai, China, in 1984 and the M.S. and Ph.D. degrees from Tsinghua University, Beijing, China, in 1987 and 1991, respectively, all in electrical engineering. He is currently a Professor and the Director of electrical engineering with Shanghai Jiao Tong University. His current research interests include application of optimization theory to power systems, power markets, and dynamic security assessment.



Venkata Dinavahi (S'94–M'00–SM'08) received the B.Eng. degree in electrical engineering from the Visveswaraya National Institute of Technology, Nagpur, India, in 1993, the M.Tech. degree in electrical engineering from the Indian Institute of Technology Kanpur, Kanpur, India, in 1996, and the Ph.D. degree in electrical and computer engineering from the University of Toronto, Toronto, Ontario, Canada, 2000. He is currently a Professor with the Department of Electrical and Computer engineering, University of Alberta, Edmonton, Alberta, Canada. His research interests include real-time simulation of power systems and power electronic systems, electromagnetic transients, device-level modeling, large-scale systems, and parallel and distributed computing.